Materials Science & Engineering A 560 (2013) 851–856

Contents lists available at SciVerse ScienceDirect

Materials Science & Engineering A

journal homepage: www.elsevier.com/locate/msea

Rapid communication

Three-dimensional printing of SiSiC lattice truss structures

Z. Fu [a], L. Schlier [a], N. Travitzky [a,b,*], P. Greil [a,b]

[a] Department of Materials Science, Glass and Ceramics, University of Erlangen-Nuremberg, Martensstrasse 5, D-91058 Erlangen, Germany
[b] Centre for advanced Materials and Processes, University of Erlangen-Nuremberg, Dr.-Mack-Strasse 81, 90762 Fuerth, Germany

ARTICLE INFO

Article history:
Received 8 August 2012
Received in revised form
11 September 2012
Accepted 14 September 2012
Available online 8 October 2012

Keywords:
Mechanical properties
SiSiC composites
Three-dimensional printing
Polymer-derived ceramics
Macrocellular lattice structure
Melt infiltration

ABSTRACT

Silicon/silicon carbide ceramic composites were fabricated by the three-dimensional printing (3DP^{TM}) from Si/SiC/dextrin powder blends. After printing the C/Si/SiC preforms were infiltrated with a liquid silicone resin for transient shape stabilization. The green bodies were pyrolyzed at 1000 °C in nitrogen atmosphere resulting in a residue with a porosity of ~41%. The porous preforms exhibit excellent infiltration behavior for liquid Si at 1500 °C in vacuum. Bending strength, fracture toughness and Young's modulus were analyzed with respect to Si volume fraction.

1. Introduction

Silicon infiltrated silicon carbide ceramics (SiSiC ceramics) are used for a wide range of engineering applications due to their excellent near-net shape fabrication and good mechanical properties combined with high chemical stability up to elevated temperatures [1–3]. SiSiC ceramics with a silicon volume fraction of 10–15% exhibit typical bending strength, fracture toughness and Young's modulus values of approximately 350 MPa, 4 MPa $m^{0.5}$ and 350 GPa, respectively [4–6]. The mechanical properties were found to scale linearly with Si-content [7].

The reactive infiltration of a porous carbonaceous preform with liquid Si (LSI-process) offers the possibility to near net-shape manufacturing of dense SiSiC composites at relative low temperatures and reasonable costs [23]. According to the LSI-process, the REFEL-process and the SILCOMP-process were developed for industrial production of SiSiC since the 70s [8–10]. It should be noted that silicon is distinguished by a volume expansion of 10% upon solidification of the melt [4,11]. The volume expansion of Si during solidification may lead to residual microstresses in the SiSiC composites [4]. In addition, due to different thermal expansion coefficients between Si and SiC, compressive residual microstresses in Si phase may arise. This microstress-induced strengthening effect may contribute to the improving mechanical properties of SiSiC ceramics [12,13].

The carbonaceous preform is commonly prepared by slip casting or cold pressing using either graphite or a mixture of carbon and α-SiC powder [14]. Macro-structures with complex geometry were fabricated by Solid-Free Form (SFF) technologies from Computer-Aided Design (CAD) data. In three-dimensional printing (3DP^{TM}) process solid objects are fabricated by layered printing, in which the sliced 2D profile of a CAD model is printed on a fresh layer of powder via deposition of a suitable binder [15]. Moon et al. [16] fabricated porous carbonaceous preforms using glassy carbon powders of 45–105 μm sizes and an acetone-based furfuryl resin binder as a printing solution. After pressureless reactive infiltration at 1450 °C in nitrogen atmosphere, a SiSiC composite with a coarse-SiC grain structure was formed [16]. Travitzky et al. [18] produced SiSiC composites from a mixture of SiC and starch–cellulose powders by 3D-printing. Dense SiSiC was obtained by subsequent pyrolysis and pressureless liquid silicon melt infiltration [18]. Yin et al. [19] built $TiAl_3/Al_2O_3$ composites by reactive infiltration of an Al melt into a porous TiO_2 preform which was prepared by indirect three-dimensional printing. Nan et al. [20] reported the near-net-shape manufacturing of Ti_3SiC_2-based ceramics by three-dimensional printing combined with liquid silicon infiltration. Schlier et al. [3] created a macrocellular lattice structure of SiSiC ceramics suitable for air–fuel mixture formation as used in automotive applications. Unbonded precursor powder served as support for ligaments with a thickness of 1.5 mm and a spacing distance exceeding 4.4 mm.

The purpose of the present work was to study the effect of Si-content on the microstructure and mechanical properties of Si–SiC composites containing a high Si fraction > 50 vol% fabricated

* Corresponding author. Tel.: +49 9131 85 28775; fax: +49 9131 85 28311.
E-mail address: nahum.travitzky@ww.uni-erlangen.de (N. Travitzky).

0921-5093/$ - see front matter © 2012 Elsevier B.V. All rights reserved.
http://dx.doi.org/10.1016/j.msea.2012.09.107

by 3D-printing. Additional liquid Si-infiltration of lattice truss structures with variable ligament lengths was carried out.

2. Experimental

Printing powder was prepared from mixtures of Si powder (Silgrain HQ 0–75 μm, Elkem ASA, Oslo, Norwegen, d_{50}=19.4 μm), α-SiC (F500D, ESK SiC GmbH, Germany, d_{50}=16.2 μm) and dextrin powder $(C_6H_{10}O_5)_n$ with n=10–200 (Superior Gelbmittel F, Suedstaerke, Schrobenhausen, Germany, d_{50}=109 μm, molecular weight 1600–32000 g/mol). The dextrin powder, which served as a binder when coming in contact with the injected water-based printer solution, was kept at a constant volume fraction of 18 vol% in all powder blends. The volume ratio between SiC and Si varied from 0/100 to 90/10, Table 1. Particle size distribution of the used powders was measured in an air stream by laser granulometry (Mastersizer 2000 APA 2000, Malvern Instruments, London, Great Britain). The process diagram for the fabrication of Si–SiC composites is shown in Fig. 1.

The powder blends were homogenized for 48 h in a tumbling mill (Reax 20, Heidolph, Schwabach, Germany) with Al_2O_3 grinding balls and sieved through 150 μm mesh before printing. 3D-printing was carried out on a 3D printer (Zprinter 310, Z-Corporation, Burlington, USA) using a water-based printing solution, containing 12.5 vol% glycerin (Glycerin Wasserfrei, Sigma Aldrich Chemie, Steinheim, Germany). Bar-shaped samples with dimension of $6 \times 7 \times 48$ mm^3 and lattice truss components were printed. The layer thickness was adjusted to 100 μm for all objects and the binder saturation was set to 0.35 g/cm^3. The lattice truss components exhibit a complex gradient geometry, where axial and radial rectangular struts with an edge length of 1.5 mm reached span length up to 45 mm.

The printed samples were dried in the powder bed at room temperature for 24 h, and subsequently cleaned from the unbound powder bed. The retrieved green bodies were then infiltrated with a liquid silicone resin, polymethylphenylhydrogensilsesquioxane $[(C_6H_5)_{0.44}(CH_3)_{0.24}(C_2H_3)_{0.16}SiO_{1.5}]_n$ (SILRES H62C, Wacker Chemie, Burghausen, Germany), which was cured by a polyaddition reaction at 130 °C for 24 h. After polymer cross-linking, the polymer infiltrated preforms showed excellent green strength and better handling performance. Pyrolysis of the preforms took place at 1000 °C for 2 h in N_2 atmosphere to ensure full decomposition of the dextrin and polysilsesquioxane. During the pyrolysis, the dextrin yielded a residual carbon content of ~25 wt%. The polysilsesquioxane was converted into an amorphous Si–O–C residue (72 wt% related to the polymer), which was composed of approximately 42 wt% of carbon. The density of the preforms was determined via helium pycnometry (Accupyc 1330, Micromeretics, Norcross, USA) and open porosity of the preforms was calculated from the measured geometrical and pycnometrical densities.

The pyrolyzed preforms were placed in a carbon crucible coated with boron nitride layer in order to prevent reaction between the carbon crucible and the Si melt. Granulated Si powder (Silgrain HQ, Elkem, Oslo, Norway) was placed around the samples to be infiltrated. The crucible was put into a vacuum furnace with 10^{-5} MPa. The infiltration temperature and time were 1500 °C and 2 h, respectively. Heating and cooling rates of 5 K/min were applied. Surfaces of the SiSiC samples were polished to a 6 μm finish prior to characterization.

Phase analysis of the infiltrated samples was conducted by X-ray diffraction (XRD, Kristalloflex D 500, Siemens, Karlsruhe, Germany) using monochromatic Cu-K_α radiation at a scan rate of 0.75 °/min over a 2θ range of 20–70°.

The microstructure of infiltrated samples was analyzed by scanning electron microscopy (SEM, Quanta 200, FEI, Prague, Czech). Prior to SEM analysis, the samples were relief-polished to a 6 μm diamond finish and sputtered with gold. Phase distribution and phase volume fraction were derived from SEM micrographs applying free image analysis software ImageJ (National Institute of Health, Bethesda, MD).

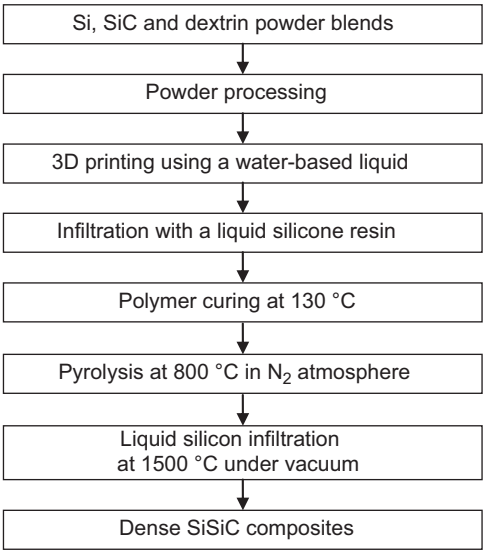

Fig. 1. Process diagram for fabrication of Si–SiC composites.

Table 1
Compositions and properties of SiSiC composites.

Volume ratio Si/SiC in starting composition	Final composition (vol%) Si	SiC	Porosity in SiSiC composites (%)	Density, ρ (g/cm^3)	Elastic modulus, E (GPa)	Elastic modulus calculated by Duckworth-equation, E (GPa)	Bending strength, σ (MPa)	Bending Strength calculated by Ondracek-equation, σ (MPa)	Fracture toughness, K_{IC} (MPa m$^{0.5}$)
10/90	51	49	0.5 ± 0.4	2.74 ± 0.02	256 ± 6	258 ± 6	208 ± 25	216 ± 26	2.5 ± 0.2
20/80	52	48	0.7 ± 0.3	2.72 ± 0.02	254 ± 3	257 ± 3	205 ± 20	217 ± 21	2.4 ± 0.1
30/70	56	44	0.8 ± 0.5	2.68 ± 0.01	237 ± 5	240 ± 5	196 ± 19	209 ± 21	2.2 ± 0.2
40/60	58	42	0.5 ± 0.3	2.67 ± 0.01	235 ± 2	237 ± 2	194 ± 23	202 ± 24	2.2 ± 0.2
50/50	60	40	1.1 ± 0.4	2.63 ± 0.02	225 ± 2	230 ± 2	183 ± 20	200 ± 22	2.0 ± 0.1
60/40	61	39	1.3 ± 0.4	2.60 ± 0.01	217 ± 3	222 ± 3	140 ± 19	156 ± 22	2.1 ± 0.1
70/30	69	31	1.4 ± 0.3	2.57 ± 0.02	207 ± 1	212 ± 1	143 ± 16	161 ± 18	1.8 ± 0.1
80/20	72	28	1.2 ± 0.8	2.52 ± 0.02	197 ± 4	201 ± 4	129 ± 15	143 ± 17	1.7 ± 0.1
90/10	76	24	5.8 ± 2.4	2.44 ± 0.03	167 ± 10	186 ± 11	71 ± 6	113 ± 10	1.2 ± 0.1
100/0	79	21	3.8 ± 1.6	2.45 ± 0.02	183 ± 7	196 ± 8	96 ± 13	130 ± 18	1.2 ± 0.1

Bending strength of the infiltrated SiSiC bars was measured by four point bending method on a universal testing device (Instron 4204, Instron Corporation, Canton, USA). The bars were loaded with spans of 20 and 40 mm at room temperature. A crosshead speed of 0.5 mm/min was applied. Average values of bending strength were calculated from at least eight measurements according to DIN EN 843-5. Fracture toughness was calculated from at least eight measurements by the single-edge-V-notched beam method (SEVNB) according to DIN CEN/TS 14425-5. A saw cut was tapered using a razor blade with 3 μm diamond paste. The overall depth of the notch was determined by light microscopy (Leica M420, Leica, Heerbrugg, Switzerland) and adjusted to about one third of the sample's height. The breaking load was measured by four point bending using spans of 10 and 20 mm to calculate the fracture toughness. Young's modulus was derived from the longitudinal sound propagation velocity measurements by an impulse excitation technique (Buzz-o-sonic, BuzzMac Software, Glendale, USA) using DIN EN 843-2 [21]. The average Elastic modulus value was determined from at least 10 measurements.

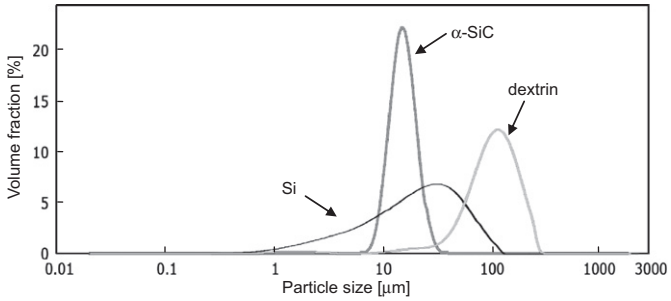

Fig. 2. Particle size distribution of Si, α-SiC and dextrin.

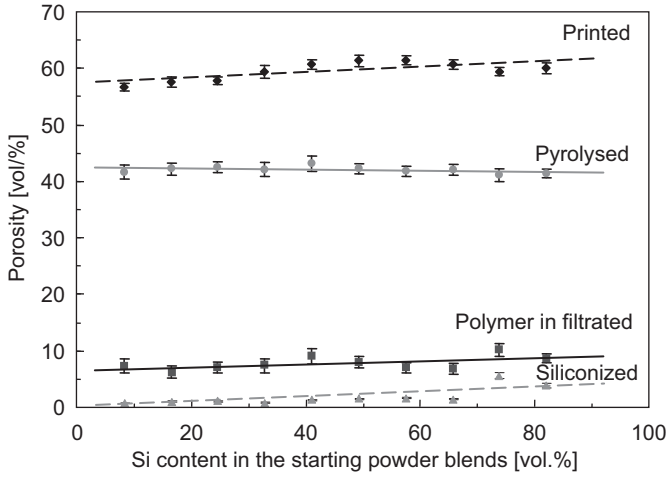

Fig. 3. Porosity of printed, polymer infiltrated, pyrolysed preforms and siliconized SiSiC ceramics as a function of Si volume fraction in the starting powder blend.

3. Results and discussion

Fig. 2 shows the particle size distribution curves of the powders. SiC and dextrin exhibit a narrow particle size distributions, while the Si powder shows a relatively broad particle size distribution. With decreasing Si content in the starting powder blends, the powder bed density rises from 1.0 g/cm^3 to 1.2 g/cm^3, and the porosity of the printed objects drops from 61.4% to 56.7%, Fig. 3. A weight increase of 40–58% was measured for the printed preforms after infiltration with the polymer. Though the liquid polymer fills the open pore system, about 8% residual porosity still remains in the polymer infiltrated preform, Fig. 4.

Fig. 5 depicts volume and linear shrinkages in three dimensions of the pyrolysed preform. Only minor differences between *x*, *y* and *z* orientation were observed which was attributed to the formation of a rigid polymer derived Si–O–C network. Thus, in contrast to pronounced difference of linear shrinkage usually observed when loosely handled printed powder components were sintered [17], shape stabilization using a preceramic polymer leads to a near net shape body with almost isotropic sintering behavior [3].

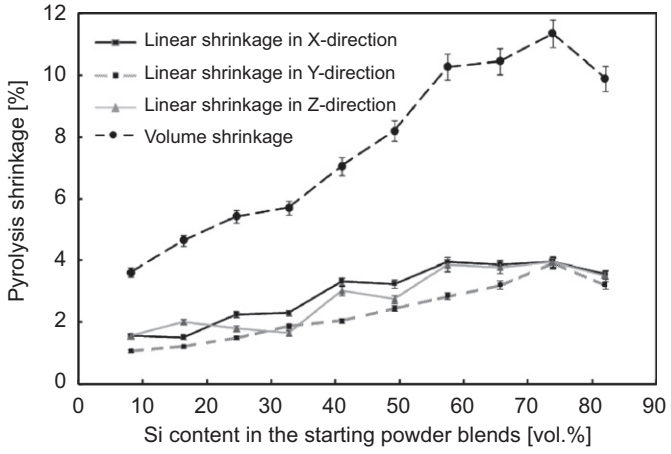

Fig. 5. Pyrolysis shrinkage as a function of Si content in the starting powder blend.

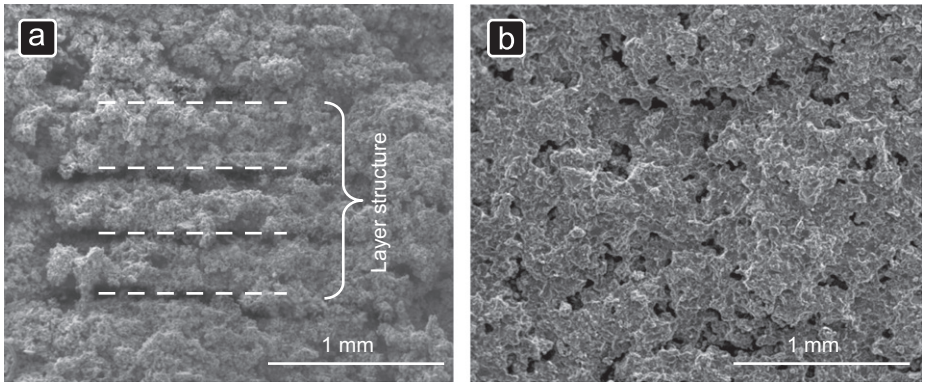

Fig. 4. SEM micrographs of a preform with starting composition of 41 vol% Si, 41 vol% SiC, and 18 vol% dextrin. (a) The layer structure of the printed samples before infiltration with silicone resin; (b) after silicone resin infiltration and polymer curing, the layered structure is hard to be recognized.

After Si melt infiltration the SiSiC composites exhibit a homogeneous and almost dense microstructure with up to 70 vol% of Si, Fig. 3. According to Washburn's equation, $d_{\max}$

$$d_{max} \approx \frac{4\gamma\cos\varphi}{\rho g h} \quad (1)$$

where γ denotes the surface tension of the melt, φ the wetting angle, ρ the density of Si melt, g the acceleration of gravity and h the infiltration height, a maximum capillary diameter d_{max} can be calculated, which limits spontaneous infiltration perpendicular to the fluid surface [24]. For the case of pressureless liquid Si infiltration at 1500 °C into a C/Si/SiC preform (γ at 1550 °C is 0.73 N/m; φ is 30° in vacuum; ρ at 1420 °C is 2.54 g/cm^3; g is 9.8 m/s^2), $d_{\max}$ of ~200 μm was found [24,25].

X-ray analysis of the fabricated composite showed the presence of α-SiC, β-SiC and Si of the first nine mixtures with lower Si content in Table 1. Elemental Si is filling the pore space and small amount of unreacted residual carbon remained, Fig. 6. The SiSiC with 0 vol% SiC in the starting composition exhibits only the Si phase and the in-situ formed β-SiC phase, Fig. 6b. Heterogeneous and homogeneous in-situ growth of secondary β-SiC grains during Si-melt infiltration is assumed, Fig. 6a. Grain sizes of SiC in the range of 2–30 μm were measured for all composites by using image analysis. Average grain sizes shifted to the higher values with an increase of SiC content in the starting composition.

After liquid Si infiltration, the first eight mixtures with lower Si content in Table 1 exhibit a dense structure with a porosity of ~1% considering possible measurement errors, Fig. 3. As illustrated in Fig. 3, only the two siliconized mixtures with higher Si content show a higher porosity of 3–5% due to the large pore sizes after pyrolysis, which are larger than the maximum infiltration capillary diameter, $d_{\max}$, Eq. (1), and cannot be filled by pressureless infiltration with Si melt. Printing of the powders with increased Si amount with fine particle size tended to spontaneous agglomeration [22], which resulted in the formation of large pores during pyrolysis [16]. The pore size distribution of different pyrolysates was measured by the intercept method according to DIN 50601, Fig. 7. The two mixtures with lower silicon content in Fig. 7 exhibit a narrow pore size distribution with maximum pore size of ~250 μm. By contrast, the two mixtures with higher silicon content have a much larger maximum pore size (> 500 μm) and show a wide pore size distribution. All pyrolysates exhibit a cumulative pore volume of ~41%, which is in good agreement with the porosity values as shown in Fig. 3.

The compositions and mechanical properties of the fabricated SiSiC composites are summarized in Table 1. In order to eliminate the effect of pores on the mechanical properties, the correct values of elastic modulus and bending strength can be calculated by Duckworth-equation [28] and Ondracek-equation [28], respectively.

The mechanical properties of multiphase materials, e.g. SiSiC ceramics, commonly can be described by the "rule of mixtures" [26]. In the case of two-phase materials, they can be calculated from the properties of each phase:

$$P = P_1 V_1 + P_2(1 - V_1) \quad (2)$$

where P represents the property of the multiphase material, V_1 the first-phase volume fraction, P_1 the property of the first phase material, and P_2 the property of the second phase. After transformation of Eq. (2) the linear relationship between P and V_1 is given by:

$$P = P_2 - (P_2 - P_1)V_1 \quad (3)$$

The density of the fabricated SiSiC composites behaves according to Eq. (3). The experimental points fall on a straight line joining the density of pure silicon (2.33 g/cm^3) and SiC (3.25 g/cm^3) [26,29], Fig. 8a, and can be described by linear equation:

$$\rho = \rho_{SiC} - (\rho_{SiC} - \rho_{Si})V_{Si}$$
$$\rho = 3.26 - 1.04V_{Si}, \quad S_\rho = 0.98 \quad (4)$$

where V_{Si} represents the Si volume fraction in the final composition of SiSiC materials and S_ρ is the correlation coefficient of the fitting curve. Equivalent linear relationships were derived for other properties [4,6,26–30], Fig. 8:

$$\text{Young's modulus}: \quad E = 398.1 - 284.7V_{Si}, \quad S_E = 0.97 \quad (5)$$

$$\text{Bending strength}: \quad \sigma = 403.2 - 360.6V_{Si}, \quad S_\sigma = 0.94 \quad (6)$$

$$\text{Fracture toughness}: \quad K_{IC} = 4.60 - 4.22V_{Si}, \quad S_K = 0.98 \quad (7)$$

A gradient macrocellular lattice truss structure was fabricated, which contains nine horizontal layers and 144 vertical struts, Fig. 9. In the first layer, 20 struts were built. Each upper layer has one strut less and larger lattice spacing than the lower layer resulting in a linear variation of strut distance and solid area

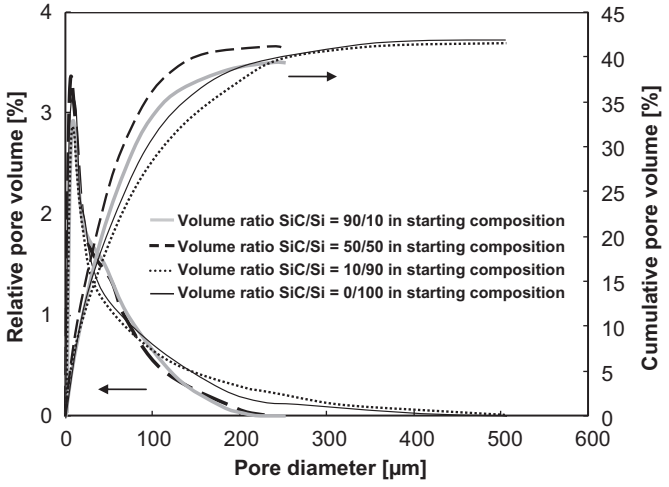

Fig. 7. Pore size distribution of different pyrolysates.

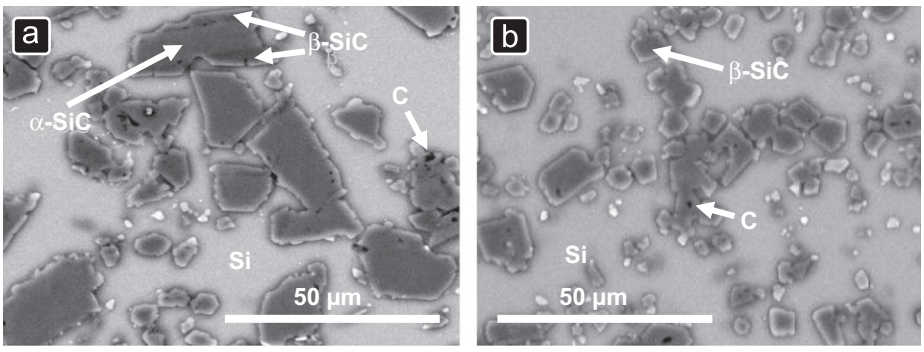

Fig. 6. Representative micrographs of the SiSiC microstructure containing (a) 82 vol% Si and (b) 57.4 vol% Si in the starting powder blend.

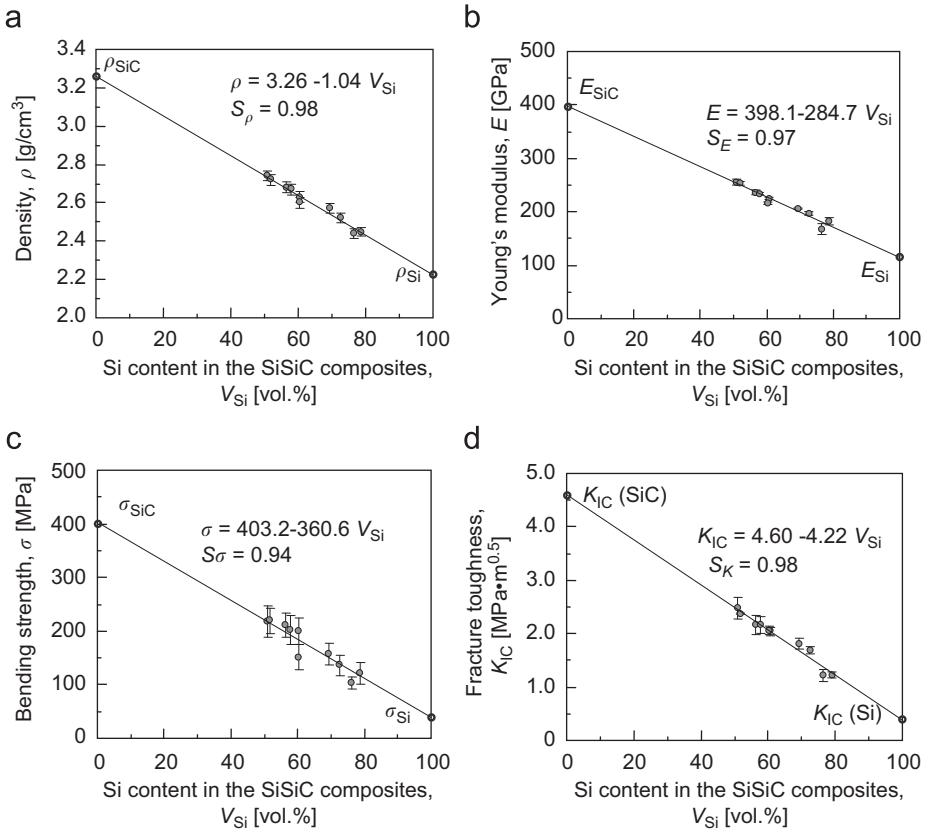

Fig. 8. Linear scaling of selected properties with Si-volume fraction measured on printed SiSiC composites.

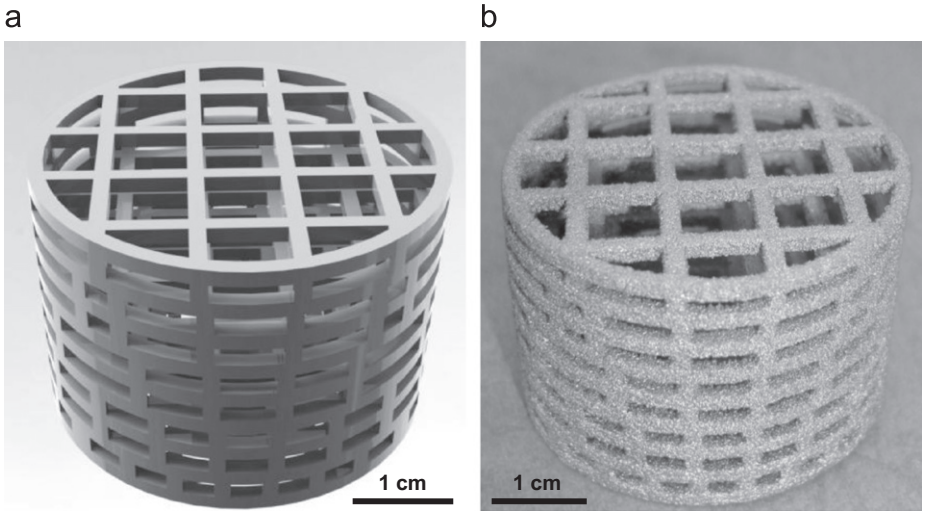

Fig. 9. Demonstration of near-net-shape capability of 3D-printing SiSiC ceramics with starting composition of 49.2 vol% Si, 32.8 vol% SiC and 18 vol% dextrin: (a) CAD design of the macrocellular lattice structure; (b) reactive-infiltrated SiSiC part.

fraction with height, Fig. 10. That means that in the last layer, the 9th layer, 12 vertical struts were built.

Infiltration depth of the silicon melt into porous struts, h, as a function of time, t, can be calculated according to [3]:

$$h = \left[t\left(\frac{V_p}{1-V_p}\right)\frac{r\gamma\cos\varphi}{6.25\eta}\right]^{1/2} \tag{8}$$

where V_p is the pore volume fraction, r is the pore radius, γ is the surface tension of the melt, φ is the wetting angle, η is the viscosity of the melt. The thickness of one layer is approximately 5 mm. For the case of pressureless liquid Si infiltration at 1500 °C into a C/Si/SiC preform with 5 mm height (V_p=0.41, η=5.5 × 10^{-4} Pas, γ=0.73 N/m, φ=30°, r=18 μm), an infiltration time of less than 1 s could be calculated [3].

The infiltration time, however, also strongly depends on the geometry of the porous body. For instance, the lattice structure in Fig. 11 contains of knots, where radial ligaments extend from the axial struts. While infiltration behavior into the lattice struts is dominated by long-range fluid transport, radial infiltration perpendicular to the major infiltration flow reduces the long-range infiltration flow [3]. For a structure containing i knots along the

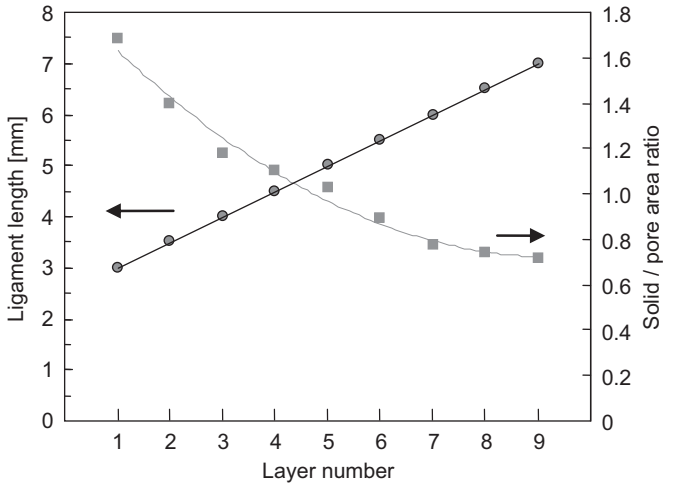

Fig. 10. Variation of strut distance and solid area fraction with the layer number of the macrocellular lattice truss structure.

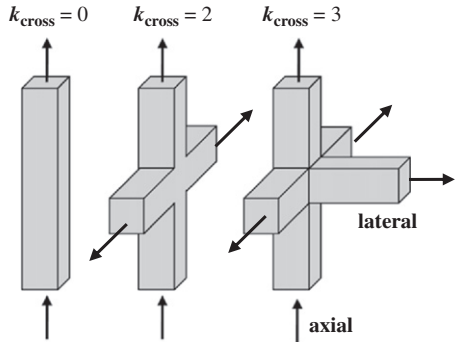

Fig. 11. Infiltration flow direction (showed by arrows) and strut geometry.

major infiltration flow (i is also the number of horizontal layer), and each knot having three radial ligament connections ($k_{cross}=3$, Fig. 11), the quotient of infiltration time of the neighbor layers can be given by:

$$\frac{t_{i+1}}{t_i} = \frac{20-i}{21-i}(k_{cross}+1), \quad i = 1,2,3\cdots 8 \tag{9}$$

where t_i represents the infiltration time up to the ith layer and t_1 can be calculated using Eq. (8). Thus t_i can be determined by:

$$t_i = t_1 \frac{21-i}{20}(k_{cross}+1)^{(i-1)}, \quad i = 1,2,3\cdots 9 \tag{10}$$

For the printed macrocellular structure, which is characterized by $i=9$, the total infiltration time of about 0.47 h is calculated which is in good agreement with the used experimental parameters.

4. Conclusions

SiSiC lattice strut structures with a gradient were fabricated by 3D printing, preceramic polymer infiltration and pressureless liquid Si infiltration. The mechanical properties of the printed SiSiC were found to be isotropic and to scale linearly with Si-volume fraction. The in-situ formed β-SiC was found to crystallize on and between primary α-SiC grains during Si-melt infiltration. The SiSiC with 18 vol% dextrin and 82 vol% Si in the starting composition exhibits only the Si phase and the in-situ formed β-SiC phase with an amount of ~21 vol%. After Si melt infiltration the SiSiC composites show a dense microstructure up to 70 vol% of Si.

Prime novelty statement

A gradient macrocellular lattice truss structure of SiSiC ceramics with complicated shape was fabricated for the first time by three-dimensional printing. The mechanical properties of the SiSiC composites with silicon content ranged from 8 to 82 vol% in the starting Si/SiC/dextrin powder blends were investigated.

Acknowledgments

Financial support from the Cluster of Excellence "Engineering of Advanced Materials" funded by DFG is gratefully acknowledged.

References

[1] J.-Y. Paris, L. Vincent, J. Denape, Comp. Sci. Technol. 61 (2001) 417–423.
[2] W. Krenkel, B. Heidenreich, R. Renz, Adv. Eng. Mater. 4 (2002) 427–436.
[3] L. Schlier, W. Zhang, N. Travitzky, P. Greil, J. Cypris, M. Weclas, Int. J. Appl. Ceram. Technol. 8 (2011) 1237–1245.
[4] H. Cohrt, Mater. Werkstofftech. 16 (1985) 277–285.
[5] L. Gmelin, R. Bohrer, G. Olbrich, 8th edition,Gmelin Handbook of Inorganic Chemistry, Silicon Supplement, vol. B3, Springer-Verlag, New York, 1986.
[6] H. Richter, G. Willmann, W. Heider, Mater. Werkstofftech. 13 (1982) 355–360.
[7] O.P. Chakrabarti, S. Gosh, J. Mukerji, Ceram. Int. 20 (1994) 283–286.
[8] P. Popper, in: P. Popper (Ed.), Special Ceramics, Academic Press, The British Ceramic Research Association, Heywood, London, 1960, pp. 209–219.
[9] C. Forrest, P. Kennedy, J. Shennan, in: P. Popper (Ed.), Special Ceramics 5, Academic Press, The British Ceramic Research Association, Stoke-on-Trent, 1972, pp. 99–123.
[10] W.B. Hillig, R.L. Mehan, C.R. Morelock, V.J. DeCarlo, W. Laskow, Am. Ceram. Soc. Bull. 54 (1975) 1054–1056.
[11] H.v. Wartenberg, Naturwissenschaften 36 (1949) 373–374.
[12] N.A. Travitzky, N. Claussen, J. Eur. Ceram. Soc. 9 (1992) 61–65.
[13] N.A. Travitzky, E.Y. Gutmanas, N. Claussen, Mater. Lett. 33 (1997) 47–50.
[14] A.J. Whitehead, T.F. Page, J. Mater. Sci. 27 (1992) 839–852.
[15] C.X.F. Lam, X.M. Mo, S.H. Teoh, D.W. Hutmacher, Mater. Sci. Eng. C 20 (2002) 49–56.
[16] J. Moon, A.C. Caballero, L. Hozer, Y. Chiang, J.C. Cima, Mater. Sci. Eng. A 298 (2001) 110–119.
[17] R. Melcher, Ph.D. Thesis, OPUS University of Erlangen-Nuremberg, Erlangen, 2009.
[18] N. Travitzky, K. Zimmermann, R. Melcher, P. Greil, Ceram. Trans. 175 (2006) 37–45.
[19] X. Yin, N. Travitzky, R. Melcher, P. Greil, Int. J. Mater. Res. 97 (2006) 492–498.
[20] B. Nan, X. Yin, L. Zhang, L. Cheng, J. Am. Ceram. Soc. 94 (2011) 969–972.
[21] M. Radovic, E. Lara-Curzio, L. Riester, Mater. Sci. Eng. A 368 (2004) 56–70.
[22] A. Aksay, C.H. Schilling, in: L.L. Hench, D.R. Ulrich (Eds.), Ultrastructure Processing of Ceramics, Glasses, and Composites, Wiley-VCH, New York, 1984, pp. 439–447.
[23] P. Greil, Mater. Chem. Phys. 61 (1999) 64–68.
[24] P. Greil, J. Eur. Ceram. Soc. 21 (2001) 105–118.
[25] P. Greil, T. Lifka, A. Kaindl, J. Eur. Ceram. Soc. 18 (1998) 1961–1975.
[26] R.L. Mehan, J. Mater. Sci. 13 (1978) 358–366.
[27] K.T. Faber, K.J. Malloy, Semiconductors and Semimetals: Mechanical Properties of Semiconductors, vol. 37, Academic Press Inc., San Diego, 1992.
[28] H. Salmang, H. Scholze, Keramik, seventh ed., Springer-Verlag, Berlin, 2007.
[29] E. Lara-Curzio, Mechanical Properties and Performance of Engineering Ceramics and Composites III, first ed., John Wiley & Sons, New Jersey, 2008.
[30] C.P. Chen, M.H. Leipold, Am. Ceram. Soc. Bull. 59 (1980) 469–472.